DOI 10.1007/s11029-022-10013-6
Mechanics of Composite Materials, Vol. 58, No. 1, March, 2022 (Russian Original Vol. 58, No. 1, January-February, 2022)

EFFECTS OF HOT-WATER AGING ON THE COMPRESSION PROPERTIES OF E-GLASS/EPOXY COMPOSITES AT VARYING STRAIN RATES

L. Gueraiche,[1*] M. Tarfaoui,[2] and H. Osmani[3]

Keywords: *glass-fiber-reinforced plastics, unidirectional reinforcement, hygrothermal effects, compressive strength, property approximation*

The effects of hot-water aging on the quasi-static and dynamic compression properties of unidirectional E-glass/epoxy laminates were investigated. E-glass/epoxy specimens were aged in water at 60°C for 4900 h and then aged and unaged specimens were tested in compression at a rate of $1.3 \cdot 10^{-3}$ s^{-1} and by a split Hopkinson pressure bar apparatus at varying strain rates. Their diffusion behavior was successfully described by the two-stage model whose parameters were found by the nonlinear regression method. The strain-rate-sensitivity of aged and unaged E-glass-reinforced epoxy specimens in the longitudinal direction was studied. Their dynamic and static compression properties were compared for specimens with the same dimensions. Empirical models were proposed to predict dynamic properties as functions of strain rate. SEM micrographs showed a low degradation of the resin matrix and fiber-matrix interface at hot-water aging for a time up to 4900 h.

1. Introduction

The composite materials used in a marine environment are subjected to impacts by other craft, floating debris, docks, and grounding and during their production [1, 2]. Therefore, it is of great importance to comprehend the effects of various environmental conditions, e.g., the hot-water aging, on the mechanical properties of composite materials under impact loadings.

Different diffusion models can be employed to explain the processes observed in glass-fiber-reinforced polymers. The simplest is the one-dimensional isotropic Fickian model [3], but deviations from it are often observed, especially for

[1]LMT, University of Jijel, 18000 Jijel, Algeria
[2]ENSTA Bretagne, IRDL - UMR CNRS 6027, F-29200 Brest, France
[3]LMNM/IOMP, University of Setif -1, 19000 Setif, Algeria
[*]Corresponding author; tel.: +213542217630; e-mail: gueraiche.larbi@univ-jijel.com

Russian translation published in Mekhanika Kompozitnykh Materialov, Vol. 58, No. 1, pp. 115-138, January-February, 2021. Russian DOI: 10.22364/mkm.58.1.07. Original article submitted July 30, 2020; revision submitted October 12, 2021.

fiber-reinforced polymers with a high void content [4]. Kumosa et al. [5] showed the behavior of unidirectional glass/epoxy composites is non-Fickian. The description of two-stage processes with diffusion- and relaxation-controlled stages proposed by Bao et al. [6] was successfully applied to the moisture absorption in epoxy/glass composites. The bulk dissolution of water in a polymer network and the moisture absorption on the surface of vacuoles were studied in [7]. A Langmuir-type model was used to predict the two-stages sorption behavior of epoxy/fiber systems [8]. This anomalous diffusion model considers the existence of mobile and bound water molecules inside the polymer network.

The sensitivity of FRP composites to the strain rate and fiber orientation was broadly investigated in the literature for unconditioned specimens. Kumar et al. [9] studied the dynamic behavior of unidirectional glass-epoxy composites at a strain rate of 265 s^{-1} for six fiber orientations (0, 10, 30, 45, 60, and 90°) using a split Hopkinson pressure bar (SHPB). All composite orientations were found to be strain-rate-sensitive. The dynamic ultimate strength exceeded the quasi-static one almost by 100% for 0, by 80% for 10° and about by 45% for all other orientations. The failure predominantly by tensile splitting occurred for the 0° orientation and by shear for other orientations. Hsiao et al. [10] used the drop weight method and a SHPB for the dynamic characterization of thick unidirectional (0 and 90) and cross-ply $\left[\left(0_8/90_8\right)_2/\overline{0}_8\right]_s$ of carbon/epoxy laminates at strain rates of up to 1800 s^{-1}. The 0° and cross-ply laminates showed the high increase in the strength and ultimate strain with increasing strain rate, but only a slight increase in the modulus. The matrix-dominated 90° laminates showed an increase in the modulus and strength, but no significant changes in the ultimate strain, with growing strain rate. Ochola et al. [11] investigated the strain-rate-sensitivity of CFRP and GFRP cross-ply [0/90] composites at strain rates of 10^{-3} and 450 s^{-1}.Their results showed an increase of the dynamic strength of GFRP with increasing strain rate . The strain to failure decreased with growing strain rate for both GFRP and CFRP specimens. Hosur et al. [12] investigated the response of unidirectional $(0)_{32}$ and $(0/90)_{16}$ cross-ply carbon/epoxy laminate composites under a high-rate compression loading using a SHPB setup at three different strain rates. The cross-ply samples were tested in the plane and across the thickness. The unidirectional samples were tested along the 0 and 90° directions. The dynamic strength, except in across-the-thickness loading of cross-ply laminates, and the stiffness exhibited considerable increase compared with the static values within the studied range of strain rates. Tarfaoui et al. [13-15] examined the effect of stacking lay-up on the in-plane dynamic compression behavior of E-glass/epoxy in the range of 200-2000 s^{-1} for fiber orientations of 0, ±20, ±30, ±45, ±60, ±70, and 90°. Their results showed a strong material sensitivity to the strain rate and fiber orientation. The failure events were different and depended on composite lay-ups. Gueraiche et al. [16] studied the dynamic compressive behavior of aged $[\pm 55]_{20}$ E-glass/epoxy laminates using a SHPB in the range of 560-1025 s^{-1}. The dynamic modulus was strain-rate-dependent, but there was a threshold effect for the ultimate strength and strain at the ultimate strength. The threshold effect was attributed to the viscoelastic nature of polymer matrix, the time-dependent nature of accumulating damage, and the considerable temperature rise in samples. The $[\pm 55]_{20}$ laminates predominantly failed by delamination, shear fracture, and splitting in several layer blocks.

Degradation of the physical properties of polymers occurs due to the combination of physical and chemical aging processes. The physical processes include plasticization, relaxation, and swelling of the polymer. The primary chemical degradation process is the hydrolysis of the polymer matrix [17]. The polar nature of the water molecule enables it to establish hydrogen bonds with the hydroxyl groups common on polymer chains, interrupting the preexisting interchain hydrogen bonds. Such modifications in the hydrogen bonding between the polymer and water molecules result in plasticization when the segmental mobility increases and swelling when the interchain bond length increases, as shown in the following equation [18]:

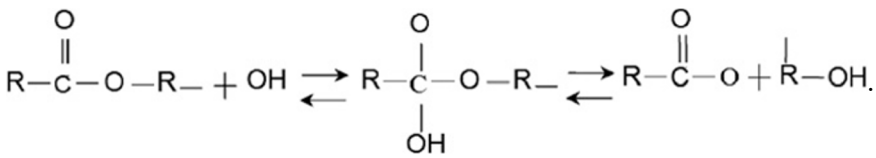

The degradation of glass fibers in water occurs by leaching and etching. The most important reaction in the dissolution of glass in water is leaching which means the diffusion of alkali ions out of the glass, as shown in the following equation [18]:

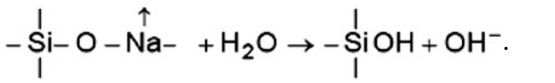

Etching is the second important reaction, in which the hydroxyl ions break Si-O-Si, as shown in the following equation [18]:

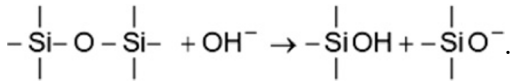

Degradation of the interphase between the fibers and matrix is complicated. Bradshaw and Brinson [19] assumed that it occurs by three damage mechanisms: matrix osmotic cracking, interfacial debonding, and delamination.

In almost all previous papers that investigated the effect of hot-water immersion and moisture on the mechanical properties of fiber-reinforced composites, it was concluded that the hot-water aging has a negative effect. Diffusion of water in polymer-matrix composites may induce swelling, plasticization, reduction of the residual strength, lowering of the glass-transition temperature T_g , and degradation of the global material performance. Soykok et al. [20] investigated the influence of hot-water aging on the tensile failure of mechanically fastened joints of glass fiber/epoxy composites. Their results showed a degradation of joint strength at higher water temperatures; the degradation was gradual with prolonged immersion times. Wosu et al. [21] studied the influence of hygrothermal aging on the through-thickness dynamic compression properties of graphite/epoxy composite materials. Both at low and high temperatures, they exhibited the sensitivity of failure properties to the strain rate at the same impact energy. It was reported that the absorbed energy linearly depended on the strain rate at low temperatures and was relatively constant at high temperatures. Nachtane et al. [22] studied the effects of hygrothermal aging on the high-strain-rate behavior of adhesively bonded composite joints. The results showed that the exposure to 50°C temperature with 80% relative humidity reduced the maximum stress with aging time in high-strain-rate loadings.

Thus, a significant amount of research has been carried out on unaged FRP composite materials at low and high strain rates and on hydrothermally aged FRP composites in quasi-static loadings. However, little or no work has been published about the experimental study of hygrothermal aging effects on the dynamic compression properties of unidirectional E-glass/epoxy laminates. Therefore, the objective of this study was to assess the effect of hot-water aging at 60°C and 4900 h on the compressive modulus, the maximum stress, and the strain at the maximum stress of unidirectional $[0]_{40}$ E-glass/epoxy (GRE) laminates at high strain in SHPB compression tests, and under quasi-static loadings using a Zwick universal testing machine. The compression properties of aged and unaged laminates were evaluated experimentally. The results obtained showed that a hot-water aging degrades the compression properties of GRE.

2. Material and Methods

2.1. Material and manufacturing process

The target unidirectional laminate $[0]_{40}$ consisted of 2400 Tex E-glass-fiber-reinforced epoxy (GRE). The Axson produced resin was prepared by mixing an EPOLAM prepolymer with an EPOLAM 2020 hardener and a 2020 accelerator. The reinforcement was a plain weave fabric with 90% warp yarns and 10% weft yarns. Unidirectional panels $[0]_{40}$ were made by the infusion process. To obtain an EPOLAM 2020 resin with a transition temperature of 80°C and the maximum mechanical properties indicated in Table 1, the panels were cured at 60°C for 16h. The square 500×500-mm panels were cut into cubic 13×13×13-mm specimens, as shown in Fig. 1. The fiber volume fraction in them, found by calcination, was about 53%.

2.2. Aging process

An Ascott climatic chamber was used to accelerate the aging of the unidirectional GRE specimens. Specimens, of 13×13×13 mm for the compression SHPB test, were submerged in a tap water at 60°C up to 4900 h. The water uptake used was the average for five specimens. In the first four days, the monitoring of water uptake was performed daily, i.e., every 24 h,

TABLE 1. Mechanical Properties of a Pure EPOLAM 2020 Resin After a Hardening Time of 16 h at 60°C or 24 h at Room Temperature

Property	Standard	Value
Flexural modulus, MPa	ISO 178 :2001	3100
Flexural strength, MPa	ISO 178 :2001	126
Tensile strength, MPa	ISO 527 :1993	78
Final hardness	ISO 868 :2003	88
Glass-transition temperature, °C	ISO 11359: 2002	80
Demolding time at room temperature without an accelerator, h	LT 051: 1998	48
Complete hardening time at room temperature, days	—	7

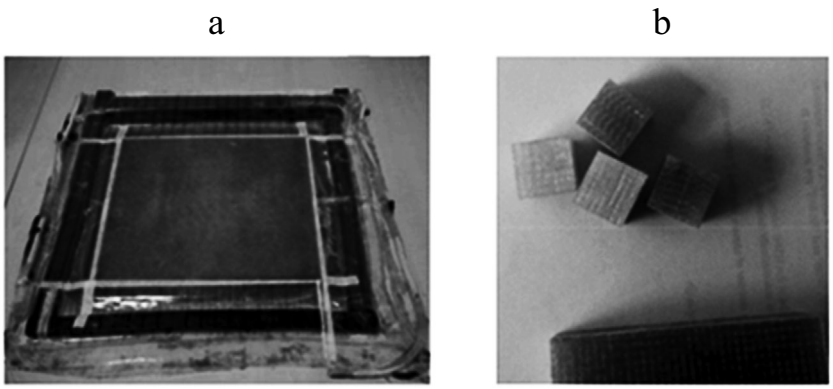

Fig. 1. Panels manufactured by the infusion process (a) and specimens (b).

and after that, it was done at regular intervals of 168 h (seven days) till 4900 h. For each water uptake measurement, the specimen was removed from the water bath, cleaned, and weighed on a precision Precisa XT220A balance (±0.1 mg). After recording the weight, the specimen was again soaked in water. The glass-transition temperature T_g of the EPOLAM 2020 resin was 80°C, which explains the choice of the 60°C aging temperature according to Gentry et al. [23], who recommended 20°C below the glass-transition temperature T_g . for the thermal aging of epoxy resins.

The content M_t of water absorbed by each specimen was calculated according to its weight before (w_0) and after exposure (w_t):

$$M_t(\%) = \frac{w_t - w_0}{w_0} \cdot 100 . \quad (1)$$

The dimensional changes of cubic specimens were measured using a caliper, by means of which changes in their length L , width W and height H could be obtained with an accuracy of 10^{-2} mm. To perform these measurements at room temperature, the samples were removed from the conditioning containers. Three samples were used to measure the dimensions of E-glass/epoxy specimens at dry and after 4900 h of hot-water aging at 60°C.

2.3. SHPB compression tests

The famous split Hopkinson pressure bar (SHPB), often called the Kolsky bar, is usually used to study the high strain-rate behavior of materials in the range of 10^2 to 10^4 s^{-1}. The SHPB apparatus of IRDL laboratory, France, used in this investigation was composed of a striker bar (0.4 m) with a rounded tip, an incident bar (1.985 m), and a transmitted bar (1.845 m),

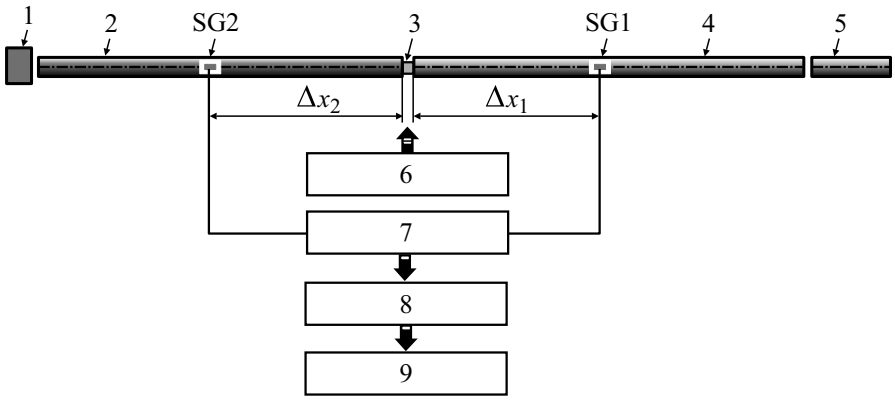

Fig. 2. An IRDL laboratory, France set-up of a split Hopkinson pressure bar: *1* — stopper; *2* — transmitted bar; *3* — specimen; *4* — incident bar; *5* — striker; *6* — high speed photography; *7* — Wheatstone bridges; *8* — Nicolet Odysey oscilloscope; *9* — computer.

as shown in Fig. 2. Three bars of 20 mm in diameter were made from a maraging steel. The striker was propelled with an initial impact velocity depending on the air gun pressure. The impact of the striker bar on the free edge of the incident bar (IB) generated a compressive stress wave that propagated through the IB to the interface incident bar/specimen. Due to the specimen-bar impedance mismatch, a part of the stress wave was reflected in the incident bar, and crossed the specimen, and went through the transmitted bar. A pair of two half Wheatstone bridges located at $\Delta x_1 = 0.9635$ m. and $\Delta x_2 = 0.959$ m from specimen/bar interfaces were used to record strain waves (Fig. 2).

The strain gage voltages were converted into incident ε_i, reflected ε_r, and transmitted ε_t strains by the equation

$$\varepsilon(t) = \frac{2.\Delta Em(t)}{k.\left(U_0 - 2\Delta Em(t)\right)} = \frac{1}{\dfrac{k.U_0}{2\Delta Em(t)} - k}, \tag{2}$$

where $\varepsilon(t), U_0, \Delta Em(t)$, and k stand for the strain, the half-bridge supply voltage, the half-bridge output voltage, and the gage factor ($k = k_{inc} = k_{trans} = 2.105$), respectively. The gages voltages were recorded using a Nicolet Odyssey 3.26 high-speed data acquisition system at a sampling rate of 1 MHz.

Six conditions have to be ensured to establish the dynamic stress–strain relationship for the SHPB [16]:

1) The bars have to remain elastic.

2) The stress wave propagation in the pressure bars is one-dimensional.

3) Specimen/bars interfaces always remain plane.

4) The inertia and friction effects in the specimen have to be reduced.

5) Strain rate has to be uniform, and the specimen stress has to be in equilibrium.

6) The specimen has to be incompressible.

After shifting the strain gage histories to specimen faces by applying the fast Fourier transform (FFT) to correct the dispersion, the engineering stress, strain rate, and strain were calculated as follows:

$$\sigma(t) = \frac{EA}{2A_s}\left[\ \varepsilon_i(t) + \varepsilon_r(t) + \varepsilon_t(t)\right] \ \text{, (3-wave analysis)} \tag{3}$$

$$\dot{\varepsilon}(t) = -\frac{2c_b}{L_s}\varepsilon_r(t), \tag{4}$$

$$\varepsilon(t) = -\frac{2c_b}{L_s}\int_0^t \varepsilon_r(t)\,dt, \tag{5}$$

where E, A, and c_b are Young's modulus, the cross-sectional area, and the speed of elastic waves in bars; L_s and A_s are the original specimen length and its cross-sectional area.

The true stress and true strain were obtained from the engineering stress and strain as follows:

$$\sigma_T(t) = \left(1 - \varepsilon(t)\right)\sigma(t), \tag{6}$$

$$\varepsilon_T(t) = -\ln\left(1 - \varepsilon(t)\right), \tag{7}$$

where $\sigma_T(t)$ and $\varepsilon_T(t)$ are the true stress and strain, respectively, $\varepsilon(t)$ and $\sigma(t)$ are the engineering stress and strain. For more details about the compression Hopkinson pressure bar set-up, assumptions of validity, delimiting pulses, and dispersion correction, see [16].

The dynamic compression tests were conducted in the plane along fibers in both aged and unaged $[0]_{40}$ GRE specimens in the range of 500-710 s^{-1}. The value of the first strain rate peak was considered in the analysis of experimental results.

The dynamic compression tests on aged specimens may be classified into low-pressure tests, which showed the elastic response with little damage, and high-pressure tests, with prevailing macroscopic damage. Based on the trial-and-error method, four pressures were chosen, i.e., a low pressure (1.3 bar), two intermediate pressures (1.5 and 1.6 bar), and the damaging pressure (2 bar), corresponding to the average strain rates of 564, 596, 606, and 663 s^{-1}. It was difficult to perform the dynamic tests on both aged and unaged specimens at the same strain rates, because they were carried out at fixed pressures. However, the impact pressures of 0.7, 0.8, and 0.9 bar allowed us to perform dynamic compression tests on unaged $[0]_{40}$ GRE specimens in the strain rate range of 500-710 s^{-1}. To ensure the reproducibility of results, at least two specimens were tested at each impact pressure. The damage history of $[0]_{40}$ GRE specimens was monitored *in situ* using a Photron Fastcam high speed camera, and the state of the specimens was illustrated after a dynamic compression loading.

2.4. Quasi-static tests

To compare the dynamic compression response with the quasi-static one, in-plane quasi-static compression tests were performed on both aged and unaged unidirectional GRE specimens, having the same dimensions as in the dynamic tests, on a Zwick universal testing machine at a constant crosshead speed of 1 mm/min ($1.3 \cdot 10^{-3}$ s^{-1}). Four tests were performed to ensure the reproducibility of results. The load–displacement response for each test was recorded using the testXpert II material testing software.

2.5. SEM characterization

A scanning electron microscope (MP12000040, UDCMA, Setif, Algeria) was used to analyze the degradation mechanisms of GRE in hot water-aging.

3. Results and Discussion

3.1. Moisture absorption and dimensional changes

Figure 3 shows the water uptake as a function of the square root of time for $[0]_{40}$ unidirectional GRE laminates. The long-term absorption data shown in Fig. 3 illustrates the two-stage diffusion, which starts with the fast Fickian diffusion followed by a slow gradual increase in the water uptake. During the first stage, the water uptake was linearly dependent on $\sqrt{t}$, which can be explained by the diffusion of water into preexisting free volume elements (defects and porosities) in the composite and the absorption of water by the epoxy resin itself [24]. The second stage characterizes polymer relaxation, involving

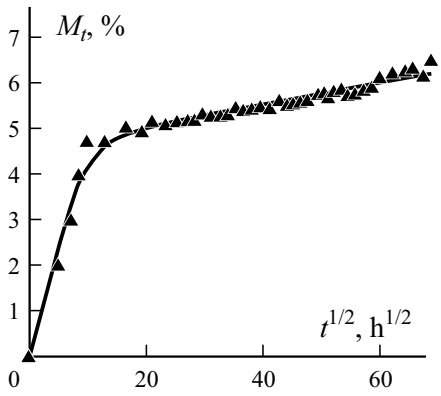

Fig. 3. Water uptake M_t versus the square root of time t for $[0]_{40}$ GRE laminates aged by immersion in a tap water at 60°C. The solid curve is the least-squares fit to experimental gravimetry data for the two-stage diffusion model (8) with $M_{\infty 0} = 4.56\,\%$, $k = 0.0053\,\mathrm{h}^{-1/2}$, $h = 0.013\,\mathrm{m}$, and $D = 3.37 \cdot 10^{-7}\,\mathrm{m}^2/\mathrm{h}$.

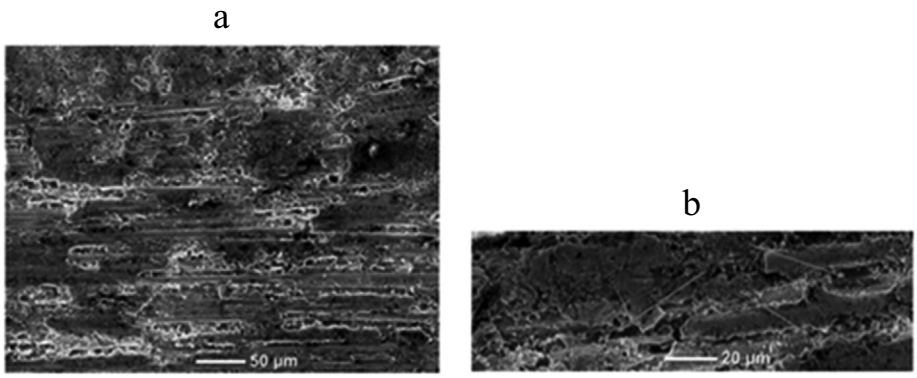

Fig. 4. SEM images of an aged $[0]_{40}$ GRE specimen: 250 (a) and 700× (b) magnifications of fracture surfaces on the front section of a SHPB test specimen showing a low deterioration of fiber-matrix interface and resin even after 4900 h of hot-water aging (a) local debondings and reduction in the amount of resin around fibers indicated by arrows (b).

a larger scale and therefore slower segmental motion, and lead to a redistribution of free-volume elements, which result in a time-dependent increase to accommodate an additional water ingress [25]. The gradual deterioration in the resin matrix and the fiber-matrix interface induced an increase in cavities, as shown in Fig. 4, and caused the unidirectional GRE specimens to keep absorbing water inside [20]. The diffusion behavior of $[0]_{40}$ unidirectional GRE laminates was successfully described by the two-stage diffusion model proposed by Bao et al. [6]:

$$M_t \approx M_{\infty 0}\left(1 + k\sqrt{t}\right)\left\{1 - \exp\left[-7.3\left(\frac{Dt}{h^2}\right)^{0.75}\right]\right\}, \tag{8}$$

where $M_{\infty 0}$ is the maximum water uptake (pseudo-equilibrium value) in the diffusion-dominated first stage. The term $\left(1 + k\sqrt{t}\right)$ characterizes the relaxation-controlled second stage, where k is related to the relaxation rate, D is diffusivity, t is time and h is specimen thickness [26, 27]. The model parameters of the two-stage diffusion recovered in the Excel using the least-squares fit to the experimental gravimetric data, are given in Fig. 3.

TABLE 2. Dimensional Changes of Samples due to Water Absorption at 60°C

Time, h	Sample No.	*L*, mm	*H*, mm	*W*, mm	Volume, mm^3
0	1	12.95	12.55	13.03	2117.67
	2	12.88	12.54	13.13	2120.69
	3	12.06	12.53	12.95	1956.90
4900	1	13.50	12.37	12.36	2064.06
	2	13.15	12.53	12.86	2118.94
	3	13.67	12.50	12.38	2115.43

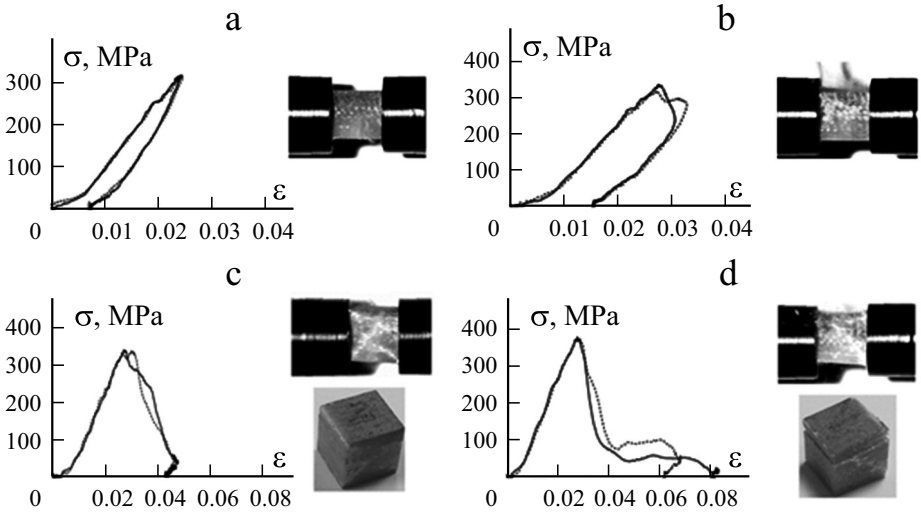

Fig. 5. Reproducibility of stress–strain curves $\sigma - \varepsilon$ and the state of unidirectional aged GRE specimens at average strain rates of 546 (a), 596 (b), 606 (c), and 663 s^{-1} corresponding to the impact pressures of 1.3, 1.5, 1.6, and 2 bar.

As seen in Table 2, the dimensional changes in the specimen lengths increased with aging time, i.e., swelling occurred along the longitudinal direction of E-glass fibers in the $[0]_{40}$ laminate, representing the favorite path for water diffusion. There was shrinkage in the transverse and through-thickness directions where fibers hindered the water diffusion. However, even there, the dimensional changes in the specimen lengths increased with water uptake.

3.2. Mechanical behavior

The dynamic tests were carried out on both aged and unaged $[0]_{40}$ GRE laminates. At each testing pressure, only a small dispersion of the stress–strain curves is seen in Figs. 5 and 6, demonstrating a good repeatability of results. The quasi-static results were included for reference.

Figure 7 illustrates the stress–strain curves of aged and unaged specimens $[0]_{40}$ GRE subjected to static and dynamic in-plane compression along the 0° orientation. The aged specimens were subjected to four impact pressures of 1.3, 1.5, 1.6, and 2 bar, corresponding to the average strain rates of 546, 596, 606, and 663 s^{-1}, as shown in Fig. 5. Each strain rate–time curve in Fig. 8a is the representative of a typical test and not the average of the tested specimens for each case. The strain rate evolution was sensitive to the impact pressure P in the air gun chamber. First, the strain rate increased rapidly for the undamaging test of 1.3 bar and then decreased and remained almost constant. The strain rate reached negative values that corresponded to the springback in the specimen. The strain rate was not constant in the second phase for the greater impact

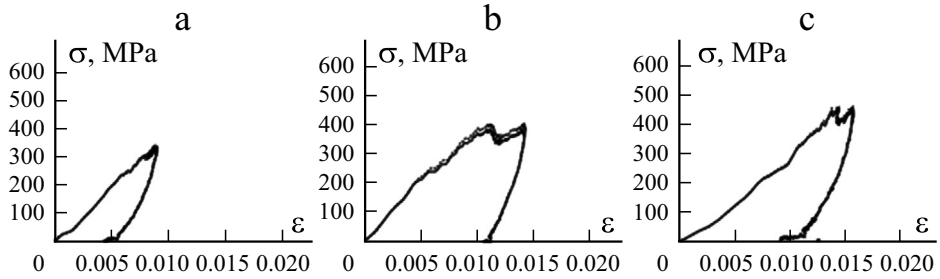

Fig. 6. Reproducibility of stress–strain curves $\sigma - \varepsilon$ for intact unidirectional unaged GRE specimens tested in dynamic compression at average strain rates $\dot{\varepsilon}$ = 519 (a), 611 (b), and 733 s^{-1} (c) corresponding to the impact pressures of 0.7, 0.8, and 0.9 bar.

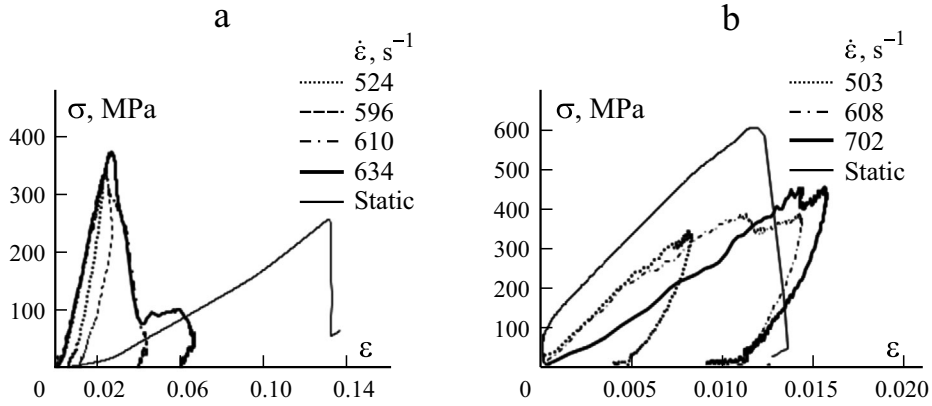

Fig. 7. Typical stress–strain curves $\sigma - \varepsilon$ of $[0]_{40}$ aged (a) and unaged (b) GRE laminates tested in the plane at various strain rates $\dot{\varepsilon}$.

pressures of 1.5 to 2 bar, as seen in Fig. 8a. The presence of the second peak in strain rate–time curves was a sign of onset of macroscopic damage [14, 15]. The critical pressure for this onset was about 1.5 bar. When the impact pressure attained 2 bar (663 s^{-1}), the second peak of strain rate versus time curve exceeded the first one; however, the springback became negligible. The main dynamic compression properties with statistics for aged and unaged $[0]_{40}$ GRE laminates subjected to the in-plane loading at various impact pressures are summarized in Table 3.

Typical stress–strain curves for static, 524, 596, 610, and 634 s^{-1} are shown in Fig. 7a. The stress–strain response of aged $[0]_{40}$ GRE laminates in dynamic loading was the same during the initial linear elastic deformation, where the compression modulus was almost insensitive to the strain rate. The dynamic stiffness of aged specimens was higher than the static one. The mean value of stiffness was 2.8 GPa for the static loading and 17.1, 17.4, 16.2, and 18.0 GPa for the rates of 546, 596, 606, and 663 s^{-1}, respectively. This suggests the presence of a stiffening mechanism when the strain rate increased from the quasi-static to the dynamic one. Such a stiffening mechanism may be related to the alteration of the progressive failure sequence that undergoes composites at low strain rates, viz. individual laminates with matrix failure followed by fiber failure [11]. The maximum stress represents the peak after which the specimen loses its load-bearing capacity. It was higher for the dynamic loading case and increased with strain rate. The mean values of maximum stress were 254 MPa for quasi-static loading and 319, 326, 341, and 373 MPa for specimens tested at 546, 596, 606, and 663 s^{-1}. The increase in the maximum stress with strain rate may be related to the shear behavior and change in failures modes [28]. The undamaging tests showed a permanent deformation that increased with strain rate. However, the specimen continued to deform in the damaging tests. Due to diverse failure modes, stress–strain curves showed different nonlinearities. The strain at the maximum stress in the static loading was higher than the dynamic one. A similar trend was also found by Ochola et al. [11]. It was suggested that, at low loading rates,

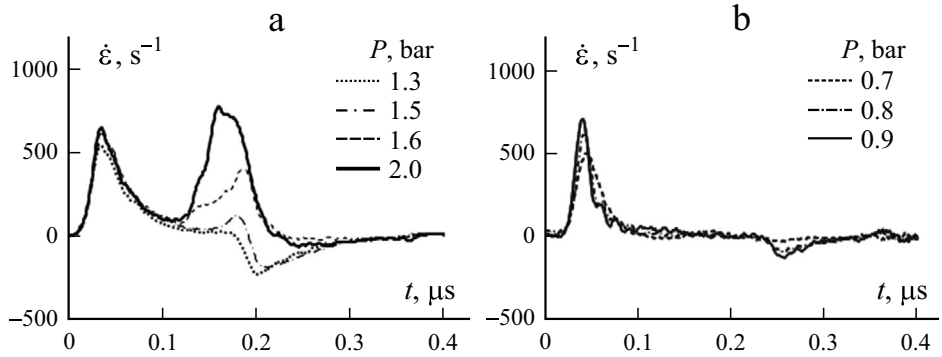

Fig. 8. Typical strain rate–time curves $\dot{\varepsilon} - t$ of $[0]_{40}$ aged (a) and unaged (b) GRE laminates tested in the plane at various impact pressures.

the GRE specimens had enough time to distribute the load and to undergo a steady deformation. However, when subjected to a rapid loading, the material tended to a more brittle behavior, resulting in a low strain at the maximum stress. The strain at the maximum stress was almost insensitive to the strain rate for aged specimens. The average strain at the maximum stress was 13.08% in the static loading and 2.49, 2.73, 2.82, and 2.71% at strain rates of 546, 596, 606, and 663 s^{-1}, respectively.

Figures 7b and 8b show typical stress–strain and strain rate–time curves of $[0]_{40}$ unaged GRE specimens in the static loading and at 503 s^{-1} (0.7 bar), 608 s^{-1} (0.8 bar) and 702 s^{-1} (0.9 bar). After the dynamic compression loading, the unaged specimens did not exhibit apparent signs of macroscopic damage, but there might be microscopic faults. The strain rate evolution was sensitive to the impact pressure. As seen in Fig. 8b, the strain rate increased rapidly up to a maximum value, which increased with impact pressure, and then decreased and remained almost constant. The springback in the specimens was almost negligeable. The SHPB dynamic compression tests were performed at fixed pressures of 0.7, 0.8, and 0.9 bar corresponding to mean rates of 519, 611, and 733 s^{-1}. To compare aged and unaged dynamic loading results, the data of unaged specimens were interpolated at the same strain rates as for the aged ones using Eqs. (10), (12), and (14), which were obtained by fitting the dynamic properties shown in Fig. 7b. The dynamic stiffness of unaged specimens was slightly higher than static one, which may be also related to the alteration of the progressive failure sequence that underwent composites at low strain rates [11]. The mean values of stiffness were 46.6 GPa in the static loading and 45.8, 53.7, and 31.8 GPa at strain rates of 519, 611, and 733 s^{-1}, respectively. The interpolated dynamic compressive modulus values of 50.1, 53.4, 53.3, and 48.2 GPa at rates of 546, 596, 606 and 663 s^{-1}, respectively, showed a slight increase-decrease trend with increasing strain rate. The static stiffness of 46.6 GPa was lower than the interpolated values of the dynamic stiffness. Unlike the aged specimens, the maximum stress of unaged specimens in dynamic loadings was lower than in the static ones. The maximum stress was 600 MPa in the quasi-static loading and 354, 385,391, and 422 MPa, respectively, at strain rates of 546, 596, 606, and 663 s^{-1}. The strain at the maximum stress in the static loading was close that in the dynamic loading at 546 s^{-1}. The strain at the maximum stress was 1.16% in the static loading and 1.07, 1.34, 1.38, and 1.54% at strain rates of 546, 596, 606, and 663 s^{-1}, respectively. Both the maximum stress and strain at the maximum stress increased for the unaged specimens with increasing strain rate.

The use of rate sensitive empirical relations allows one to get reliable data for engineering utilizations in modeling the dynamic response of composite materials. The best fits to in-plane dynamic compression properties versus strains data of the [0]40 GRE composite allowed as to propose the following nonlinear constitutive empirical models:

$$E_c = 23.58\text{E}-05\dot{\varepsilon}^2 - 0.278\dot{\varepsilon} + 98.7, \qquad \text{aged} \tag{9}$$

$$E_c = -12.4\text{E}-04\dot{\varepsilon}^2 + 1.483\dot{\varepsilon} - 390, \qquad \text{unaged} \tag{10}$$

$$\sigma_{max} = 31.75\text{E}-04\dot{\varepsilon}^2 - 3.37\dot{\varepsilon} + 1211.7, \qquad \text{aged} \tag{11}$$

$$\sigma_{max} = 350.4ln\left(\dot{\varepsilon}\right) - 1854.3, \quad \text{unaged} \tag{12}$$

TABLE 3. Dynamic Compression Properties of Aged and Unaged $[0]_{40}$ GRE Laminates Subjected to In-Plane Loading at Various Impact Pressures

Test No	$L\times W\times H$, mm	P, bar	$\dot{\varepsilon}$, s^{-1}	E_c, GPa	σ_{max}, MPa	$\varepsilon_{\sigma_{max}}$, %
			Unaged samples			
1	12.61×12.51×13.87	0.7	503	45.2	341	0.88
2	12.87×12.73×13.54		535	46.4	331	0.87
Average			519	45.8	336	0.88
STDEV.P			16	0.6	5	0.01
1	12.11×12.42×13.32	0.8	608	49.6	384	1.40
2	12.34×12.69×13.66		614	57.7	403	1.41
Average			611	53.7	394	1.41
STDEV.P			3	4.0	10	0.01
1	11.91×12.38×13.52	0.9	702	31.6	451	1.55
2	12.63×12.56×13.11		763	31.9	462	1.56
Average			734	31.8	457	1.56
STDEV.P			31	0.2	6	0.01
			Aged samples			
1	13.23×13.13×12.73	1.3	524	17.2	317	2.36
2	13.19×13.01×12.78		567	17.1	321	2.62
Average			546	17.1	319	2.49
STDEV.P			22	0.0	2	0.13
1	13.31×13.00×12.70	1.5	597	18.5	335	2.75
2	13.09×13.35×12.71		595	16.2	317	2.70
Average			596	17.4	326	2.73
STDEV.P			1	1.2	9	0.02
1	13.42×13.10×12.80	1.6	611	15.9	342	2.71
2	13.00×13.14×12.74		601	16.5	340	2.92
Average			606	16.2	341	2.82
STDEV.P			5	0.3	1	0.10
1	13.15×13.08×12.60	2	692	17.8	376	2.76
2	13.08×13.03×12.70		634	18.3	370	2.66
Average			663	18.0	373	2.71
STDEV.P			29	0.2	3	0.05

$$\varepsilon_{\sigma_{max}} = -5.39\text{E}-05\dot{\varepsilon}^2 + 0.0671\dot{\varepsilon} - 18.08, \quad \text{aged} \tag{13}$$

$$\varepsilon_{\sigma_{max}} = -2.12\text{E}-05\dot{\varepsilon}^2 + 0.0297\dot{\varepsilon} - 8.83. \quad \text{unaged} \tag{14}$$

3.3. Failure modes

A Photron FASTCAM high-speed camera was used to monitor the damage history of specimens. The Photographs and the Photron real-time-taken images in Fig. 5 show the failure modes of unidirectional GRE specimens after in-plane dynamic compression loadings. The macroscopic damage onset was detected by the presence of the second peak in the strain rate versus

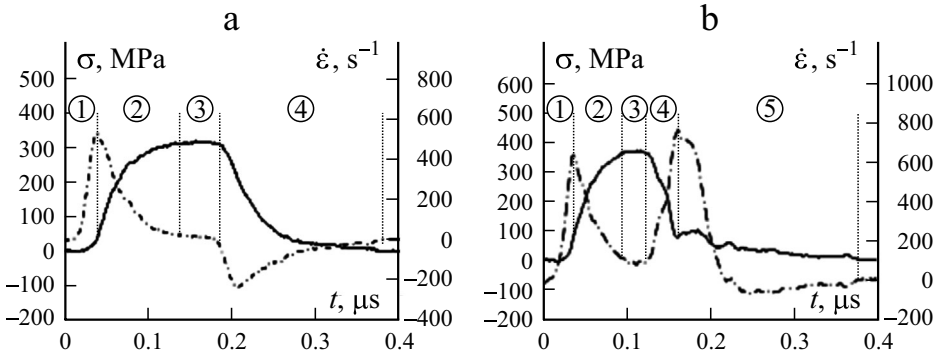

Fig. 9. Stress $\dot{\sigma}$ and strain rate $\dot{\varepsilon}$ vs. t time curves of [0]40 unidirectional GRE specimens. (a) P = 1.3 bar (524 s^{-1}), undamaging test and (b) P =2 bar (634 s^{-1}), damaging test. The solid lines are stress–time curves and the dash-dotted ones are strain rate–time curves.

time curve, which corresponded to the fall of stress in the specimen, as shown in Fig. 9. From the stress and strain rate versus time curves in Fig. 9, various zones can be distinguish, which can be summarized as follows [14]:

a) For nondamaging tests, Fig. 9a

- Zone 1. This zone is characterized by a fast evolution of strain rate $\dot{\varepsilon}$, which can be interpreted by the self-installation of samples between the bars. Indeed, the parallel sample faces in contact with the bars was not 100% guaranteed the considerations of clearance and only a slight nonlinear increase in the stress in this zone.

- Zone 2. Since a perfect contact was ensured, the strength of material induced an increase in σ and a drop in $\dot{\varepsilon}$.

- Zone 3. Evolution of σ translated the incidental signal evolving around an average value with $\dot{\varepsilon}$ tending towards a zero value. When $\dot{\varepsilon}$ tended to zero, the sample reached the maximum compression under the maximum stress.

- Zone 4. In this zone, $\dot{\varepsilon}$ changed the sign, but σ started to decrease; the specimen began to relax. This behavior can be explained by the specimen springback, which was found by an analysis of stereotypes taken by high-speed photography. At the end of this zone, both signals were cancelled at the same time.

b) For damaging tests, Fig. 9b.

- Zone 1. Similar observations as in zone 1 in nondamaging tests.

- Zone 2. The same as for zone 2 in nondamaging tests.

- Zone 3. The evolution of stress represents the dynamic compression with a constant average value of σ and $\dot{\varepsilon}$. In this zone, where σ reaches its maximum value, the fluctuations were more marked than in the nondamaging test. This phenomenon can be explained by the appearance of damage on a microscopic level.

- Zone 4. The accumulation of microscopic damage involved the appearance of macroscopic defects, which induced a rapid fall in the stress with a rapid increase in $\dot{\varepsilon}$.

- Zone 5. The damaged specimen became more compact, which causes a sharp drop in $\dot{\varepsilon}$. In this zone, σ always decreased, but less markedly than in zone 4. The appearance of damage caused the attenuation of springback behavior or their disappearance if the specimen was totally damaged.

The main failure modes unidirectional GRE specimens subjected to quasi-static loading were fiber microbuckling, kinking, crashing, shear failure and delamination. The prominent was the shear failure mode, which is typical of brittle materials undergoing the transverse tension due to the Poisson ratio effect.

In dynamic loading, failure modes changed with growing strain rate. At 1.3 bar (546 s^{-1}), the unidirectional aged GRE specimens underwent a permanent strain of 9.5‰ without an apparent macroscopic damage (Fig. 7). As the compression evolved and the impact pressure reached 1.5 bar (596 s^{-1}), the aged specimens exhibited whitening due to the initiation of microscopic damage. The size and incidence of damage became more significant with impact pressures increasing to 1.6 bar (606 s^{-1}), when the prevailing failure mode was the shear fracture across the diagonal and from opposite corners. On the up-right side, the shear fracture induced the separation of external layers in the block (Fig. 5c). At 2 bar (663 s^{-1}), specimens

TABLE 4. In-Plane Compression Properties of Aged and Unaged $[0]_{40}$ GRE Laminates with Change Percentage Due To Hot-Water Aging at Various Strain Rates: Static, 546, 596, 606, and 663 s^{-1}

$\dot{\varepsilon}$, s^{-1}	E_c, GPa			σ_{max}, MPa			$\varepsilon_{\sigma_{max}}$, %		
	Unaged	Aged	Δ, %	Unaged	Aged	Δ, %	Unaged	Aged	Δ, %
Статика	46.6	2.8	–94.0	600	254	–57.7	1.16	13.08	1027.6
546	50.1	17.1	–65.9	354	319	–9.9	1.07	2.49	132.7
596	53.4	17.4	–67.4	385	326	–15.3	1.34	2.73	103.7
606	53.3	16.2	–69.6	391	341	–12.8	1.38	2.82	104.3
663	48.2	18.0	–62.7	422	373	–11.6	1.54	2.71	76.0

failed by the shear fracture of layers along the diagonal, followed by a macroscopic delamination that separated the upper external layers and induced the collapse of specimens by forming a near Y shape, as illustrated in Fig. 5d.

The unaged unidirectional specimens remained intact and did not exhibit any macroscopic damage up to 663 s^{-1}. However, there might appear a microscopic fault. The damage evolution of $[0]_{40}$ unaged GRE specimens was studied by Tarfaoui et al. [14] at up to 1.6 bar, and damage was found to arise at 1.2 bar.

3.4. Effect of hot-water aging on the quasi-static and dynamic compression properties

The hot-water aging was expected to reduce the dynamic compression response of GRE laminates [20, 29]. In this work, the effect of hot-water aging on the quasi-static and dynamic properties of $[0]_{40}$ GRE specimens was investigated by comparing results of compression properties of unaged and aged specimens tested at various strain rates. The main compression properties of $[0]_{40}$ GRE composites are summarized in Table 4 and shown in Fig. 10. The quasi-static results were included in Table 4 for reference.

The degradation of GRE composites under hot-water aging can mainly be attributed to the deterioration of the matrix, of the fiber-matrix interface, or of both.

As shown in Table 4, a considerable softening occurred in the stiffness of $[0]_{40}$ GRE laminates under the hot-water aging. The compressive modulus reduced by 94.0% in the static loading and by 65.9, 67.4, 69.6, and 62.7% at strain rates of 546, 596, 606, and 663 s^{-1}, respectively. The decrease in the compressive modulus can be related to the plasticizing effect of water (6.52%), which increased the mobility of epoxy resin [30].

As shown in Table 4, the maximum stress due to the hot-water aging reduced less pronouncedly in the dynamic loading than in the quasi-static one. The decrements of the maximum stress for the aged specimens relative to the unaged were 57.7% in the static loading and 9.9, 15.3, 12.8, and 11.6% at strain rates of 546, 596, 606, and 663 s^{-1}, respectively. The fair weakening of $[0]_{40}$ GRE laminates under dynamic loading was attributed to the low deterioration of epoxy matrix and GRE interfacial bonding, as shown in Fig. 4.

In the static loading, the aged specimens showed higher strains at the maximum stress than in the dynamic loading. The aged specimens underwent higher strains at the maximum stresses than the unaged ones, as shown in Table 4.

4. Conclusions

This paper presents results of an experimental investigation into the effect of hot-water aging on the dynamic and quasi-static compression properties of $[0]_{40}$ E-glass/epoxy (GRE) laminates. The laminates were aged in water at 60°C for 4900 h. Compression split Hopkinson pressure and quasi-static tests were performed on aged and unaged unidirectional GRE laminates. The following conclusions can be drawn from the results of the current study:

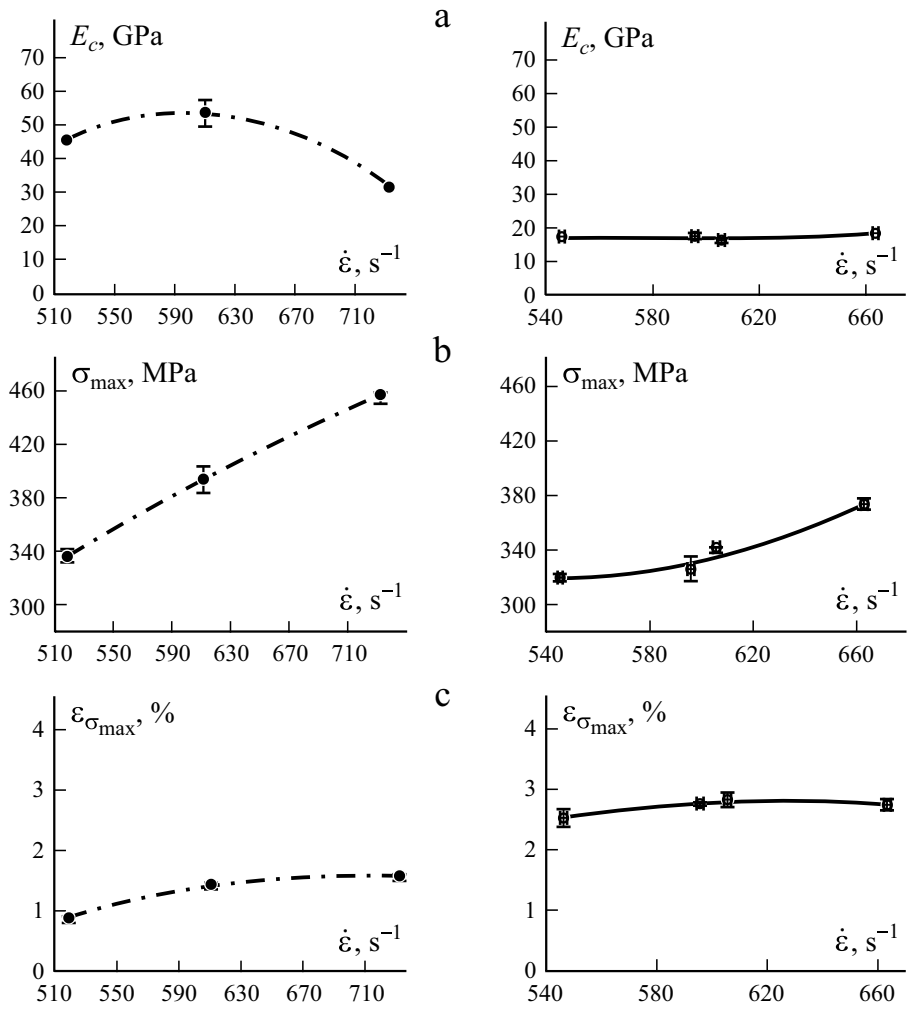

Fig. 10. The effect of hot-water aging on the compression modulus E_c (a), maximum stress σ_{max} (b), and strain $\varepsilon_{\sigma_{max}}$ (c) at the maximum stress fitted to the data of aged (○) and unaged (●) $[0]_{40}$ GRE laminates by solid and dash-dotted lines, respectively.

The diffusion behavior of $[0]_{40}$ unidirectional GRE laminates was successfully described by the two-stage diffusion model. At 4900 h, the water uptake reached 6.52%. The parameters of the two-stage model were determined using the non-linear regression method.

Dimensional changes showed a swelling along the longitudinal direction of E-glass fibers, representing the favorite path for water diffusion, and a shrinkage in the transverse and through-thickness direction, where fibers hindered the water diffusion. Even there, the relation between the water uptake and the dimensional change in the longitudinal direction of fibers was linear.

The dynamic properties, such as the compressive modulus, the maximum stress, and the strain at the maximum stress, of aged and unaged $[0]_{40}$ composites were sensitive to the strain rate. Empirical models were proposed to assess the dynamic properties at strain rates of 546-663 s^{-1} to facilitate the design and optimization of such structures without recourse to an experimental investigation, which requires a long time and money to obtain reliable data for an engineering use in modeling the dynamic response.

The failing process of hot-water aging of unidirectional GRE laminates was monitored using a Fastcam high-speed camera. At 1.6 bar (610 s^{-1}), the prevailing fracture mode was the shear banding with several white bands. At 2 bar (634 s^{-1}), the prominent failure modes were the shear banding and delamination.

SEM micrographs showed that the property degradation of unidirectional GRE laminates in hot-water aging can be mainly attributed to deterioration of the epoxy matrix and the GRE interface.

The compressive modulus reduced in were by 94.0% in the static loading and by 65.9, 67.4, 69.6, and 62.7% at strain rates of 546, 596, 606, and 663 s^{-1}, respectively. The decrements of the maximum stress for the aged specimens relative to the unaged ones were 57.7% in the static loading and 9.9, 15.3, 12.8, and 11.6% at strain rates of 546, 596, 606, and 663 s^{-1}, respectively. In the static loading, the aged specimens showed higher strains at the maximum stress than in the dynamic loading. The aged specimens underwent higher strains at the maximum stresses than the unaged ones. The increments of strain at the maximum stress due to the hot-water aging were 1027.6% for static loading and 132.7, 103.7, 104.3, and 76% at strain rates of 546, 596, 606, and 663 s^{-1}, respectively. This precise and reliable assessment of the percentage of changes in the quasi-static and dynamic compression properties under hot-water aging can help designers to establish the life-cycle "knock-down" factors for composite structures made of unidirectional $[0]_{40}$ E-glass/epoxy laminates.

Acknowledgements. This research was funded by the General Directorate of Scientific Research and Technological Development- DGRSDT (MESRS) of Algeria.

REFERENCES

1. L. Sutherland, "A review of impact testing on marine composite materials: part iii-damage tolerance and durability," Compos. Struct., **188**, Mar., 512-518 (2018).
2. F. Rubino, A. Nisticò, F. Tucci, and P. Carlone, "Marine application of fiber reinforced composites: A review," J. Mar. Sci. Eng., **8**, No.1, 26 (2020).
3. Y. Joliff, L. Bélec, and J. F. Chailan, "Modified water diffusion kinetics in an unidirectional glass/fibre composite due to the interphase area: Experimental, analytical and numerical approach," Compos. Struct., **97**, Mar., 296-303 (2013).
4. B. D. Harper, G. H. Staab, and R. S. Chen, "A note on the effects of voids upon the hygral and mechanical properties of AS4/3502 graphite/epoxy," J. Compos. Mater., **21**, No.3, 280-289 (1987).
5. L. Kumosa, B. Benedikt, D. Armentrout, and M. Kumosa, "Moisture absorption properties of unidirectional glass/polymer composites used in composite (non-ceramic) insulators," Compos. Part Appl. Sci. Manuf., **35**, No. 9, 1049-1063 (2004).
6. L.-R. Bao, A. F. Yee, and C. Y.-C. Lee, "Moisture Absorption and hygrothermal aging in a bismaleimide resin," Polymer, **42**, No. 17, 7327-7333 (2001).
7. J. J. M. Machado, E. A. S. Marques, A. Q. Barbosa, and L. F. da Silva, "Effect of hygrothermal aging on the quasi-static behaviour of CFRP joints varying the overlap length," Compos. Struct., **214**, Apr., 451-462 (2019).
8. H. G. Carter and K. G. Kibler, "Langmuir-type model for anomalous moisture diffusion in composite resins," J. Compos. Mater., **12**, No. 2, `118-131 (1978).
9. P. Kumar, A. Garg, and B. Agarwal, "Dynamic compressive behaviour of unidirectional gfrp for various fibre orientations," Mater. Lett., **4**, No. 2, 111-116 (1986).
10. H. M. Hsiao, I. M. Daniel, and R. D. Cordes, "Dynamic compressive behavior of thick composite materials," Exp. Mech., **38**, No. 3, 172-180 (1998).
11. R. O. Ochola, K. Marcus, G. N. Nurick, and T. Franz, "Mechanical behaviour of glass and carbon fibre reinforced composites at varying strain rates," Compos. Struct., **63**, No. 3, 455-467 (2004).
12. M. Hosur, J. Alexander, U. Vaidya, and S. Jeelani, "High strain rate compression response of carbon/epoxy laminate composites," Compos. Struct., **52**, No. 3-4, 405-417 (2001).
13. M. Tarfaoui and M. Nachtane, "Staking lay-up effect on dynamic compression behaviour of E-glass/epoxy composite materials: Experimental and numerical investigation," Adv. Mater. Lett., **9**, No. 11, 816-822 (2018).
14. M. Tarfaoui, A. Nême, and S. Choukri, "Damage kinetics of glass/epoxy composite materials under dynamic compression," J. Compos. Mater., **43**, No. 10, 1137-1154 (2009).

15. T. Mostapha, in : Brahim Attaf (eds.), Experimental Investigation of Dynamic Compression and Damage Kinetics of Glass/Epoxy Laminated Composites under High Strain Rate Compression, Ch.16, Advances in Composite Materials - Ecodesign and Analysis, IntechOpen Limited, London, UK (2011).
16. L. Gueraiche, M. Tarfaoui, H. Osmani, and A. Aboulghit El Malki, "A practical note for SHPB test with new algorithms for delimiting pulses," Compos. Struct., **126**, Aug., 145-158 (2015).
17. M. K. Antoon and J. L. Koenig, "The structure and moisture stability of the matrix phase in glass-reinforced epoxy composites," J. Macromol. Sci. Part C, **19**, No. 1, 135-173 (1980).
18. Y. Chen, J. F. Davalos, I. Ray, and H.-Y. Kim, "Accelerated aging tests for evaluations of durability performance of FRP reinforcing bars for concrete structures," Compos. Struct., **78**, No. 1, 101-111 (2007).
19. R. D. Bradshaw and L. C. Brinson, "Physical aging in polymers and polymer composites: An analysis and method for time-aging time superposition," Polym. Eng. Sci., **37**, No. 1, 31-44 (1997).
20. I. F. Soykok, O. Sayman, and A. Pasinli, "Effects of hot water aging on failure behavior of mechanically fastened glass fiber/epoxy composite joints," Compos. Part B Eng., **54**, Nov., 59-70 (2013).
21. S. Wosu, D. Hui, and L. Daniel, "Hygrothermal effects on the dynamic compressive properties of graphite/epoxy composite material," Compos. Part B Eng., **43**, No. 3, 841-855 (2012).
22. M. Nachtane, M. Tarfaoui, S. Sassi, A. El Moumen, and D. Saifaoui, "An investigation of hygrothermal aging effects on high strain rate behaviour of adhesively bonded composite joints," Compos. Part B Eng., **172**, Sept., 111-120 (2019).
23. T. Gentry, L. Bank, A. Barkatt, and L. Prian, "Accelerated test methods to determine the long-term behavior of composite highway structures subject to environmental loading," J. Compos. Technol. Res., **20**, No. 1, 38-50 (1998).
24. S. Ma, Y. He, L. Hui, and L. Xu, "Effects of hygrothermal and thermal aging on the low-velocity impact properties of carbon fiber composites," Adv. Compos. Mater., **29**, No. 1, 55-72 (2020).
25. A. R. Berens and H. B. Hopfenberg, "Diffusion and relaxation in glassy polymer powders: 2. Separation of diffusion and relaxation parameters," Polymer, **19**, No. 5, 489-496 (1978).
26. L.-R. Bao and A. F. Yee, "Moisture diffusion and hygrothermal aging in bismaleimide matrix carbon fiber composites-part I: Uni-weave composites," Compos. Sci. Technol., **62**, No. 16, 2099-2110 (2002).
27. J. Zhang, X. Cheng, X. Guo, J. Bao, and W. Huang, "Effect of environment conditions on adhesive properties and material selection in composite bonded joints," Int. J. Adhes. Adhes., **96**, Jan., 102302 (2020).
28. H. M. Hsiao and I. M. Daniel, "Strain rate behavior of composite materials," Compos. Part B Eng., **29**, No. 5, 521-533 (1998).
29. J. Wang, H. GangaRao, R. Liang, and W. Liu, "Durability and prediction models of fiber-reinforced polymer composites under various environmental conditions: A critical review," J. Reinf. Plast. Compos., **35**, No. 3, 179-211 (2016).
30. P. Nogueira, C. Ramirez, A. Torres, M. J. Abad, J. Cano, J. Lopez, I. López-Bueno, and L. Barral, "Effect of water sorption on the structure and mechanical properties of an epoxy resin system," J. Appl. Polym. Sci., **80**, No. 1, 71-80 (2001).